Acquisition of the Wide Swath Significant Wave Height From HY-2C Through Deep Learning

Jichao Wang[1], Ting Yu[1], Fangyu Deng[1], and Yongjun Jia[2]

[1]China University of Petroleum
[2]National Satellite Ocean Application Service

November 30, 2022

Abstract

The significant wave height (SWH) is of great importance in industries such as ocean engineering, marine resource development, shipping and transportation. Haiyang-2C (HY-2C), the 2nd operational satellite of China's marine dynamic exploration series, can provide all-weather, all-day, global observations of wave height, wind, and temperature. In this paper, a deep learning approach is applied to build a wide swath model based on the SWH from the altimeter and the wind speed from the scatterometer of HY-2C. Two validation sets, 1-month data at 6-minute intervals and 1-day data with an interval of 10 s, are fed into the trained model. Experiments indicate that the extending nadir SWH yields a real-time wide swath grid product along track, which can be offered as support for oceanographic study, and it is superior to take the swell characteristics of ERA5 into account as the input of wide swath SWH model. In conclusion, the verification results demonstrate the effectiveness and feasibility of the wide swath SWH model.

Acquisition of the Wide Swath Significant Wave Height From HY-2C Through Deep Learning

J. C. Wang[1], T. Yu[1], F. Y. Deng[1], and Y. J. Jia[2*]

[1]College of science, China University of Petroleum, Qingdao 266580, Shandong, China.

[2]National Satellite Ocean Application Service, Beijing 100081, China.

Corresponding author: Y. J. Jia (jiayongjun@mail.nsoas.org.cn)

Key Points:

- The nadir significant wave height (SWH) is extended to wide swath SWH.
- A deep learning network is built using wave and wind observed simultaneously by HY-2C, which yields a real-time and along-track product.
- The swell and wind wave from ERA5 are respectively added as input, and the swell produces superior validation results.

Abstract

The significant wave height (SWH) is of great importance in industries such as ocean engineering, marine resource development, shipping and transportation. Haiyang-2C (HY-2C), the 2nd operational satellite of China's marine dynamic exploration series, can provide all-weather, all-day, global observations of wave height, wind, and temperature. In this paper, a deep learning approach is applied to build a wide swath model based on the SWH from the altimeter and the wind speed from the scatterometer of HY-2C. Two validation sets, 1-month data at 6-minute intervals and 1-day data with an interval of 10 s, are fed into the trained model. Experiments indicate that the extending nadir SWH yields a real-time wide swath grid product along track, which can be offered as support for oceanographic study, and it is superior to take the swell characteristics of ERA5 into account as the input of wide swath SWH model. In conclusion, the verification results demonstrate the effectiveness and feasibility of the wide swath SWH model.

Plain Language Summary

The wider spatial coverage of significant wave height (SWH) can provide more information and data support. Haiyang-2C (HY-2C) can acquire Ku-band SWH from altimeter and wind speed from scatterometer at the same time to provide a basis for marine disaster prevention and mitigation, marine scientific research, etc. In this paper, a gate recurrent unit (GRU) neural network is used to build a wide swath model with the data provided by HY-2C and ERA5. Different input features are employed to train and verify the model. The wide swath SWH provides wider, orbit tracking and real-time grid datasets, which can advance further studies, such as wave assimilation, spatial-temporal prediction, extreme analysis and so on. The swell of ERA5 has a positive effect on the wide swath SWH modeling process and performs well, which could be a promising choice when real-time standard is not strictly required.

1 Introduction

Significance wave height (SWH) is the most widely utilized wave parameter in climate assessment and various marine industries. Buoys are traditional measurement tools of SWH that can provide comprehensive information and are studied extensively in researches (Guenaydin 2008; Lin et al., 2020; Kang et al., 2021). However, its disadvantages of single-point measurements with sparse and limited coverage no longer meet the needs of the rapid development of economic, military and scientific research fields, thus wider spatial coverage is of general interest.

Satellite altimeters can quickly and accurately measure the global sea surface height, and their measurement accuracy has reached the centimeter level. The measured SWH form Geosat radar (Dobson, 1987), Jason-1 and Envisat (Durrant et al., 2009), SARAL/AltiKa (Bhowmick et al., 2015; Mahesh Kumar et al., 2015; Sepulveda et al., 2015), Sentinel 3A and 3B (Yang and Zhang, 2019; Yang et al., 2020), Haiyang-2 series (Wang et al., 2013; Chen et al., 2013; Zhang et al., 2015; Wang et al., 2020), Chinese-French Oceanography Satellite (CFOSAT) (Liang et al., 2021; Li et al., 2021) altimeter are validated by comparison with those of the National Data Buoy Center. For such data, the path is still equivalent to a one-dimensional time series, which greatly limits the number of observations.

Haiyang-2C (HY-2C), China's third marine dynamic environment satellite, is subordinate to the HY-2 marine remote sensing satellite series. HY-2C combines visible/infrared and microwave sensors, with high-precision orbit measurement, orbit determination capabilities, and

all-weather, all-day, and global detection capabilities. Thus, it provides support services for marine resources development, marine environmental protection, and national defense construction, etc.

Deep learning is a class of efficient algorithms for learning representative and discriminative input features in a hierarchical manner (Zhang et al., 2016), which has become a hot topic in various fields, particularly in marine remote sensing, such as classifying oceanographic objects from Synthetic Aperture Radar (SAR) data (Bentes et al., 2016), retrieving sea surface wind speed in SAR images (Shen, et al., 2019; Qin et al., 2021), providing higher accuracy SWH for wave assimilation (Wang et al., 2021; Wang et al., 2021), etc. It is worth noting that Wang et al. (2020) developed a deep learning approach for retrieving the SWH over an extended swath via a CFOSAT with simultaneous wind and wave observations. As a matter of fact, we attempt to find a more specific deep neural network using fewer input features to retrieve a wider swath of SWH. The gate recurrent unit (GRU) network is designed to solve the gradient disappearance problem that occurs in standard recurrent neural network, and is a popular and creditable choice because of its simple structure, fast training speed, and dominant effect.

In this paper, we adopt a deep learning method to obtain a wide swath of SWH from simultaneous observations of radar altimeter (ALT) and microwave scatterometer (SCA) of HY-2C. First, the nadir SWH obtained by ALT is employed to select the wind speed of SCA, where the time difference is less than 5 s, and we spatially choose the closest wind column. Approximately eight months (from Sep. 25, 2020 to Jun. 1, 2021) of the HY-2C and ERA5 collected datasets are considered and matched. In the configuration cases, the matching criteria are set within 100 km for geographical distance and half an hour for temporal difference. Then the validation set is divided by a length of 300, and the statistical results are analyzed through the leftmost, center and rightmost columns located in the wide swath SWH, in order to illustrate the performance of the wide swath SWH model in each segmented interval. Finally, the results of the 1-day validation set at 10-second intervals are discussed, and two small areas are selected and drawn separately to demonstrate the validation effect of the wide swath SWH model at different ranges of numerical variation.

The structure of this paper can be summarized as follows: Section 2 introduces the characteristics of HY-2C and ERA5, as well as adopted method and datasets. Section 3 compares and analyzes the performance of the model. Finally, Section 4 concludes this paper.

2 Data and Method

Haiyang-2C (HY-2C) was successfully launched on September 21, 2020 at the Jiuquan Satellite Launch Center in Inner Mongolia, China. Unlike the HY-2B satellite in a polar orbit, the HY-2C satellite operates in an inclined orbit (Pang and Tao, 2016), which travels at an altitude of 1336 km and presents an orbital inclination angle of 66°. Thus, it achieves the purpose of accelerating satellite revisit to the area within 70 degrees north south form the equator, shortening the observations interval of the region, and improving the observations efficiency. HY-2C, the first large-scale inclined orbit remote sensing satellite, was constructed under the National Civil Space Infrastructure Plan (Ren, 2020). The satellite adopts an orbit with regression periods of 10 and 400 days in the early and later stage, respectively.

The main function of the ALT is to measure the global sea surface height, SWH and gravity field parameters, with sea and land observations capabilities, and the ALT has an external calibration working mode that can cover the complete calibration area. Its operating frequency

denotes13.58 GHz, 5.25 GHz, pulse limited footprint is better than 2 km, and the range accuracy of marine nadir point is better than 2 cm. Although the HY-2C ALT provides SWH in Ku and C bands, we select only Ku-band measurements as experimental data in this paper due to its higher accuracy, and the fact that the C-band is designed mainly to modify the path delay caused by ionosphere during Ku-band ALT (Jia et al., 2020).

HY-2C carries a Ku-band rotating pencil-beam SCA in a non-sun-synchronous orbit. As the main payload of marine dynamic environment, SCA has a coverage rate of not less than 90% in the global sea area for 1 to 2 days. Its main function is to measure the wind vector field (**Figure 1**), and the accuracy of wind direction and wind speed measurement are better than 15° and 1.5 m/s, respectively. It also has an external calibration working mode with an operating frequency of 13.256 GHz and two beams, which are HH polarization for the internal beam and VV polarization for the external beam. Moreover, Wang et al. (2021) verified the wind product of the SCA and believed its great availability.

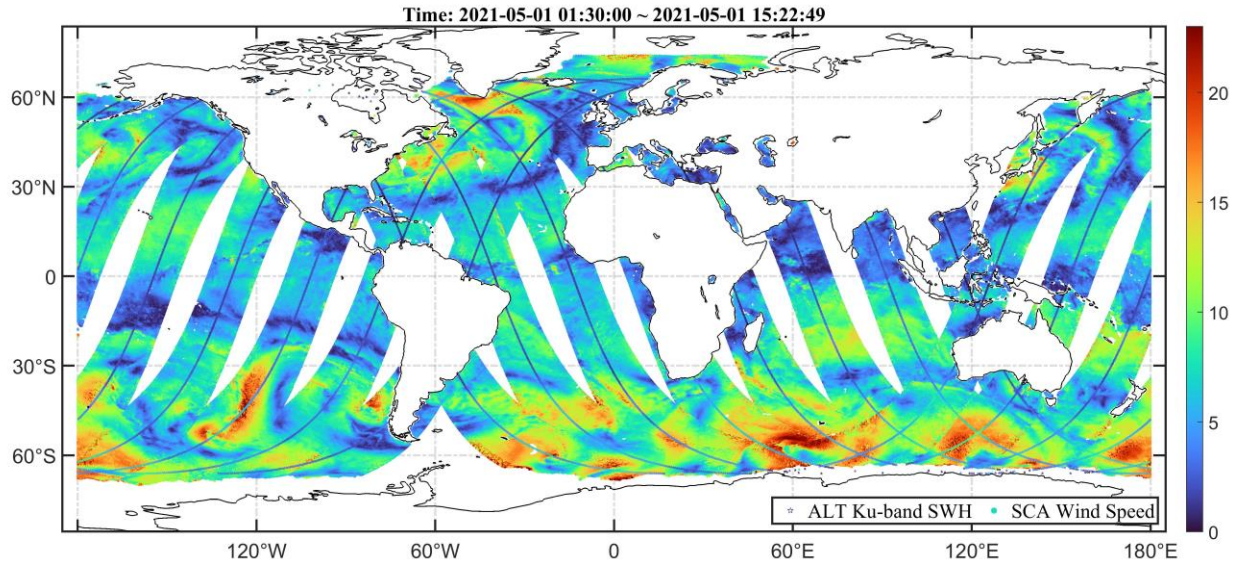

Figure 1 Information of the wind speed from SCA and the Ku-band SWH from ALT are obtained simultaneously from HY-2C on May 1, 2021.

ERA5 is a global climate reanalysis datasets released by the European Center for Medium-Range Weather Forecasts. It has the advantages of high spatial resolution, hourly atmospheric, terrestrial and ocean climate variables, 3-hourly uncertainty information, more satellite observations, and accessing to all input observations (Hersbach et al., 2020). The collected SWH has a resolution of 0.25° longitude by 0.25° latitude in space and hourly in time.

The wind and wave from remote sensing data and the wave from analysis datasets have different types of property, and they are regarded as necessary features and labels for purpose of verifying the effectiveness of the data. Therefore, the SWH of ERA5 are compared with the observations of HY-2C ALT, the wind speed of ERA5 are by contrast with SCA L2B product, as shown in **Figure 2**.

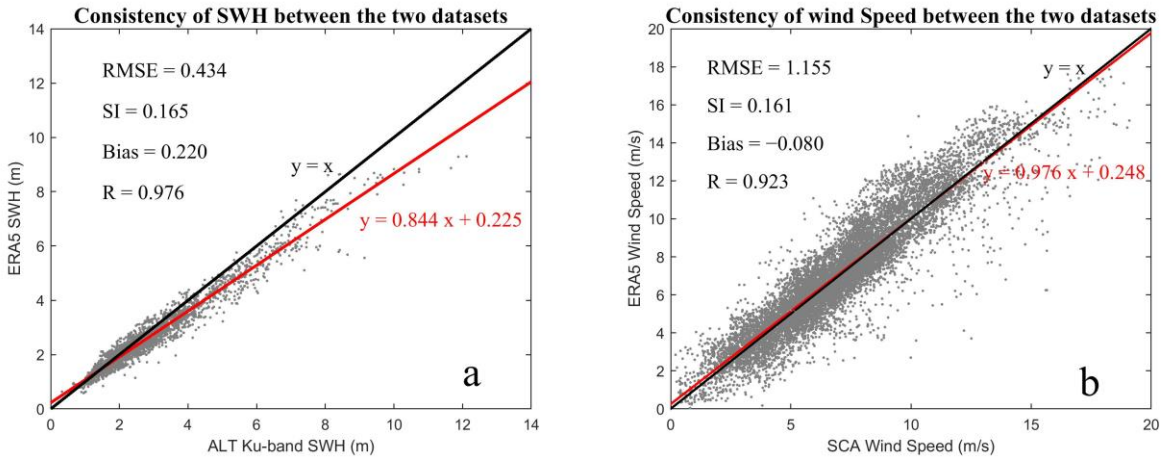

Figure 2 Scatter plots of SWH (a) and wind speed (b) from HY-2C and ERA5 to check the consistency. The red line indicates a linear fit and the black line means a full correlation.

It can be seen that both SWH and wind speed show great consistency, indirectly indicating that it is reasonable to use matched ERA5 SWH as labels at the space and time scales, further proving the feasibility of the model. The statistical metrics, namely, root mean square error (RMSE), scattering index (SI), bias (Bias), and the Pearson correlation coefficient (R), are applied to measure the effectiveness of the data and model, defined as follows.

$$RMSE = \sqrt{\frac{1}{N}\sum_{t=1}^{N}(y_o^t - y_v^t)^2}$$

$$SI = RMSE/mean(y_o)$$

$$Bias = \sum_{t=1}^{N}(y_o^t - y_v^t)$$

$$R = \frac{\sum_{t=1}^{N}\left(y_o^t - mean(y_o)\right)\left(y_v^t - mean(y_v)\right)}{\sqrt{\sum_{t=1}^{N}\left(y_o^t - mean(y_o)\right)^2}\sqrt{\sum_{t=1}^{N}\left(y_v^t - mean(y_v)\right)^2}}$$

where y_v^t and y_o^t are validation and observations, respectively.

Deep learning approaches can be capable of handling various problems and have been widely applied in various directions. Its attached GRU model possesses two unique gating devices, the reset gate r_t and the update gate z_t, to make a selection between the input x_t and the state of hidden layer unit at the previous moment h_{t-1}, enabling the model to preserve important features in the long-term sequence. Intuitively speaking, the reset gate r_t determines the chosen characteristics of combining x_t with h_{t-1}, and the update gate z_t defines the information saved from the candidate state $\tilde{h}_t$ to the current moment hidden state h_t (**Figure 3a**). The GRU model consists of five layers of neurons. The weights and biases between the neurons are iterated and updated during the training process, using the adaptive moment estimation optimizer and the mean square error loss function as supervision to create a wide swath model. The main parameters of the model are the batch size, the number of hidden layers, the number of hidden units per layer, the learning rate and iterations, which take the values of 20, 3, 20, 0.001, and 500, respectively.

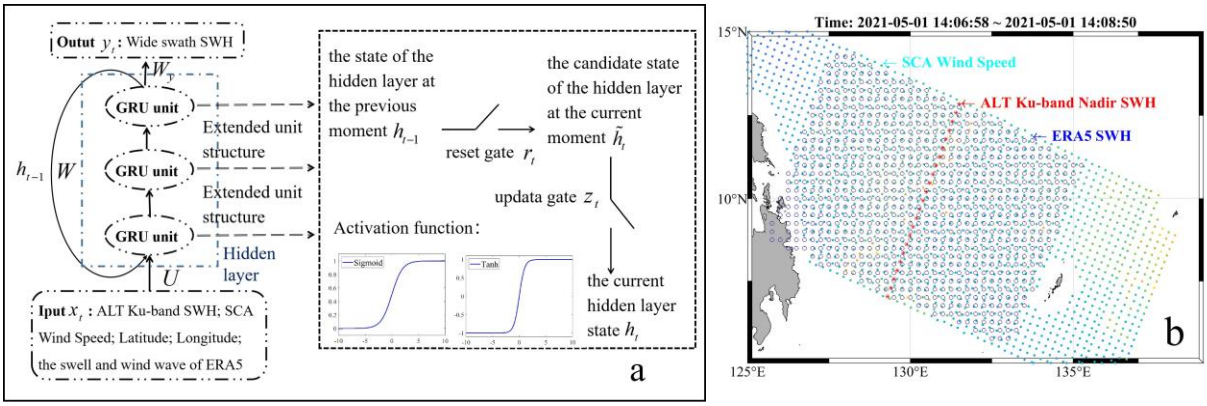

Figure 3 (a). The structure diagram of the GRU network to obtain the wide swath SWH. (b). A schematic diagram of the data parameters and widths acquired by the ALT, SCA, and ERA5. It is worth noting that the widths displayed by ERA5 are selected according to comprehensive consideration of model efficiency and effectiveness.

To make width of the nadir SWH close to the dimension of SCA wind speed, different parameters are considered as inputs, including the nadir SWH, latitude, and longitude acquired by ALT, the wind speed collected by SCA L2B product, as well as swell, wind wave, and SWH obtained by ERA5. We first give the nadir SWH at six-minute intervals and apply their geographical location and corresponding moment for the selection of the derived wind speed. Wind speed and SWH are acquired on different instruments at the same time, but the presence of missing data requires the latter to be employed as a reference to filter the former using the time difference no more than 5 s (**Figure 3b**). In addition, the distance between the SCA grid and matched data by ERA5 is limited to less than 100 km, the time window denotes ±30 min, and the width of the matched SWH account for half of the wind field in accordance with the efficiency and benefit. The latitude range is selected between 60° S and 60° N due to the validity and large probability distribution of the data. The scope of the training data set is from September 25, 2020 to April 25, 2021 for half a year, while the validation data set represents independent one-month with the time range from May 1, 2021 to June 1, 2021.

3 Results and analysis

Wide-dimensional fields have more information and data volume. We utilize the wind speed and SWH simultaneously retrieved by HY-2C as features and the SWH obtained by ERA5 as labels, so that a wide swath model can be built. It is well known that the ALT data are generated almost per second. Based on the dual consideration of runtime and the amount of data, we extract the nadir SWH at six-minute intervals and filter the data with a length of 15,360 samples in the training set. While for the validation set, we execute the same operation with an integration length of 2500 observations. The swell and wind wave information in ERA5 has a certain effect on the building of wide swath SWH model, for which we gather the relevant data after matching based on the latitude and longitude of the nadir SWH, and apply them as the input features of Experiments 2 and 3, respectively. The other parameters and settings remain unchanged. The processed datasets are fed into the GRU model, thereby the validation set results are shown in **Table 1**.

186 **Table 1** Numerical results of the validation set in the GRU model with different input features.

Input features of experiments 1-3	RMSE	SI	Bias	R
Experiment 1: Wind and SWH simultaneously acquired by HY-2C, Latitude, and Longitude	0.4056	0.1528	0.0154	0.9428
Experiment 2: Wind and SWH simultaneously acquired by HY-2C, Latitude; Longitude, and Swell obtained from ERA5	0.3696	0.1381	-0.0069	0.9530
Experiment 3: Wind and SWH simultaneously acquired by HY-2C, Latitude, Longitude, and Wind wave collected from ERA5	0.4344	0.1629	0.0032	0.9353

187

188 **Table 1** depicts that the swell presents a positive influence on the establishment of wide
189 swath SWH model, on the contrary, the wind wave has a negative impact on it. For example,
190 compared to RMSE of the Experiment 1, that of the Experiment 2 decreases 0.0360 m, which
191 indicates that the model performance is improved, while that of the Experiment 3 increases 0.0288
192 m, implying more inefficient the model output. Wind wave mainly exhibits sharp peak, which is
193 prone to wave breaking when the wind remains strong, while swell presents smoother, with long
194 and regular wave lines. The wide swath SWH model concentrates on long-term features in the
195 process of learning wind and wave characteristics, while for wind wave, it behaves as local
196 features. Overall, we mainly focus on the first two experiments in the following analysis.

197 Three columns of data with a length of 300 on the leftmost, center, and rightmost sides of
198 wide swath SWH are selected as representatives to further analyze the performance of different
199 stages. In **Table 2**, the three columns numerical results of Experiment 1 are shown that the center
200 column has better results than the other two columns under arbitrary segmented data. The reason
201 for this phenomenon may be that the larger the distance between both sides of the nadir SWH and
202 the center, the less the importance of the wind in the modeling process, and the worse the effect on
203 the nadir SWH.

204 In the segmented data, the validation results of the three columns for Interval 1 are the
205 worst among those for all intervals. For Interval 5, its leftmost and rightmost columns show
206 superior values, its center column is excellent and second only to the center column for Interval 4.
207 We count the total number of points with SWH less than 1 m (troughs) and greater than 7 m (peaks)
208 for each phase. Results indicate that Interval 1 has 332 minimal and maximal points, and these
209 local features gradually disappear during the process of training, resulting in inferior performance.
210 Surprisingly, Interval 5 has only 85 extreme points, thus dominates the results. Based on the above
211 analysis, Interval 5 (bolder words in **Table 2**), which locates in the middle of validation set and
212 remains superior, is selected to display the range and validation results of the three columns of data,
213 as shown in **Figure 4**.

214

215

216

217

Table 2 The numerical results of the segmented data on the leftmost, center, and rightmost columns in Experiment 1.

Segmented data in the validation set		RMSE	SI	Bias	R
Interval 1: 1-300	The leftmost column	0.6785	0.2633	0.0210	0.8449
	The center column	0.6023	0.2319	-0.0079	0.8931
	The rightmost column	0.7392	0.2813	-0.0524	0.8280
Interval 2: 301-600	The leftmost column	0.4650	0.1740	-0.0277	0.9280
	The center column	0.2577	0.0966	0.0351	0.9797
	The rightmost column	0.5155	0.1928	-0.0018	0.9041
Interval 3: 601-900	The leftmost column	0.4632	0.1725	-0.0038	0.9335
	The center column	0.2862	0.1064	0.0323	0.9779
	The rightmost column	0.4687	0.1716	-0.0160	0.9333
Interval 4: 901-1200	The leftmost column	0.4623	0.1734	0.0580	0.9293
	The center column	0.2420	0.0891	-0.0137	0.9820
	The rightmost column	0.4484	0.1623	-0.0239	0.9453
Interval 5: 1201-1500	**The leftmost column**	**0.4289**	**0.1680**	**0.0244**	**0.9180**
	The center column	**0.2554**	**0.0996**	**0.0221**	**0.9731**
	The rightmost column	**0.4155**	**0.1591**	**0.0197**	**0.9279**
Interval 6: 1501-1800	The leftmost column	0.4712	0.1776	0.0426	0.9037
	The center column	0.2844	0.1072	0.0308	0.9688
	The rightmost column	0.4954	0.1843	-0.0100	0.9100
Interval 7: 1800-2100	The leftmost column	0.4438	0.1711	0.0528	0.9128
	The center column	0.2673	0.1034	0.0175	0.9662
	The rightmost column	0.5030	0.1906	-0.0454	0.8819
Interval 8: 2101-2400	The leftmost column	0.5086	0.1875	0.0737	0.9323
	The center column	0.2798	0.1026	0.0610	0.9763
	The rightmost column	0.4834	0.1758	0.0446	0.9268

Comparing **Figure 4a-c**, it can be found that the center column can evaluate the peaks, while SWH on the leftmost and rightmost columns are generally underestimated at the peaks and slightly overestimated at the troughs, which are consistent with the experimental results obtained in **Table 2**. Although the red line is not as good as the blue line in **Figure 4b** for some peaks, it has a better fit between 1 and 5 m. To summarize, the results of the segmented interval in the three columns of data has an acceptable performance, understanding the effectiveness of the model. To distinctly demonstrate the accuracy of the model, the validation results for 1 day (from May 1 to May 2, 2021) with 10-second intervals are plotted in **Figure 5**.

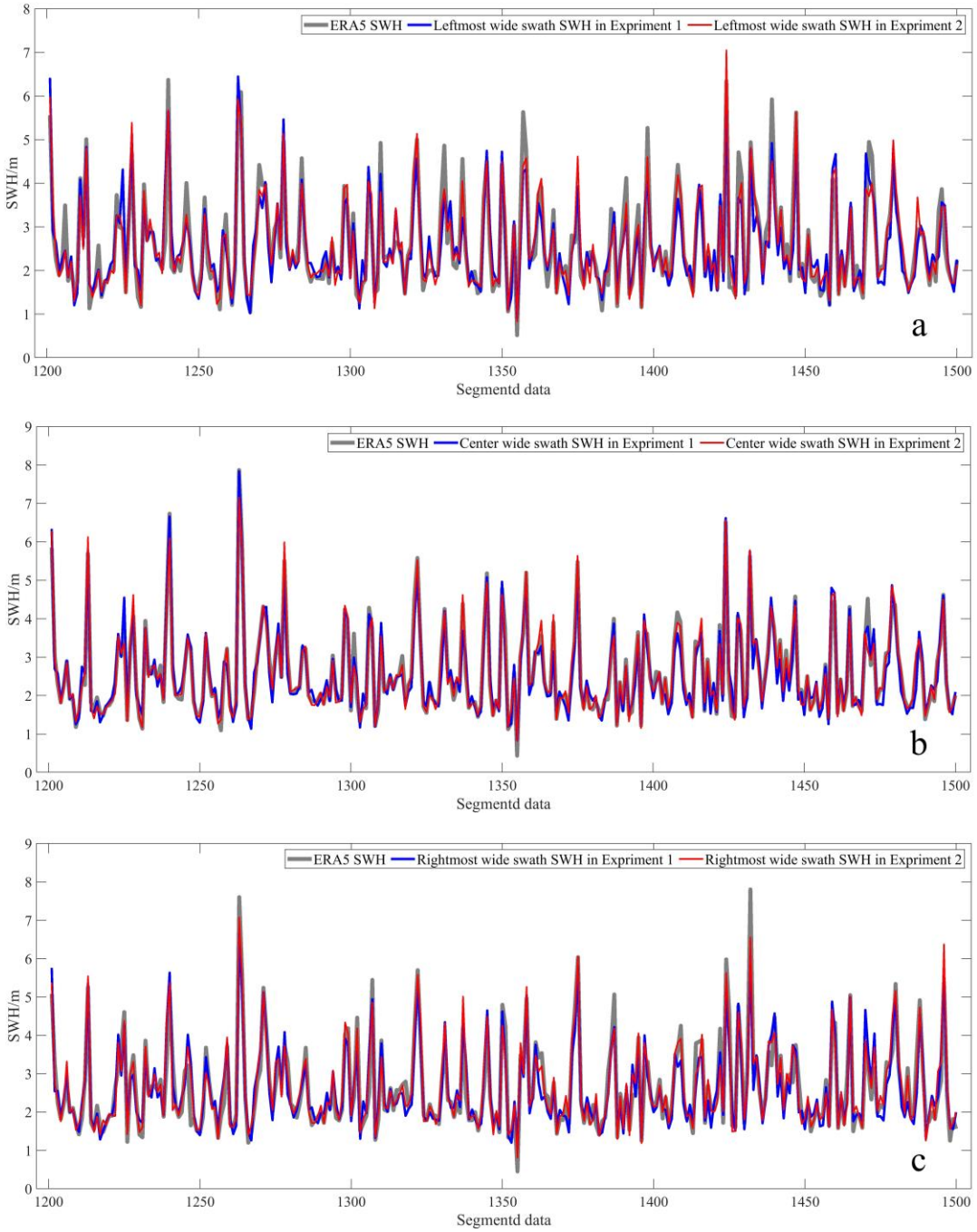

Figure 4 The line graphs of the segmented data. The leftmost, center and rightmost validation results of Experiments 1 (blue lines) and 2 (red lines) are denoted in a-c, respectively.

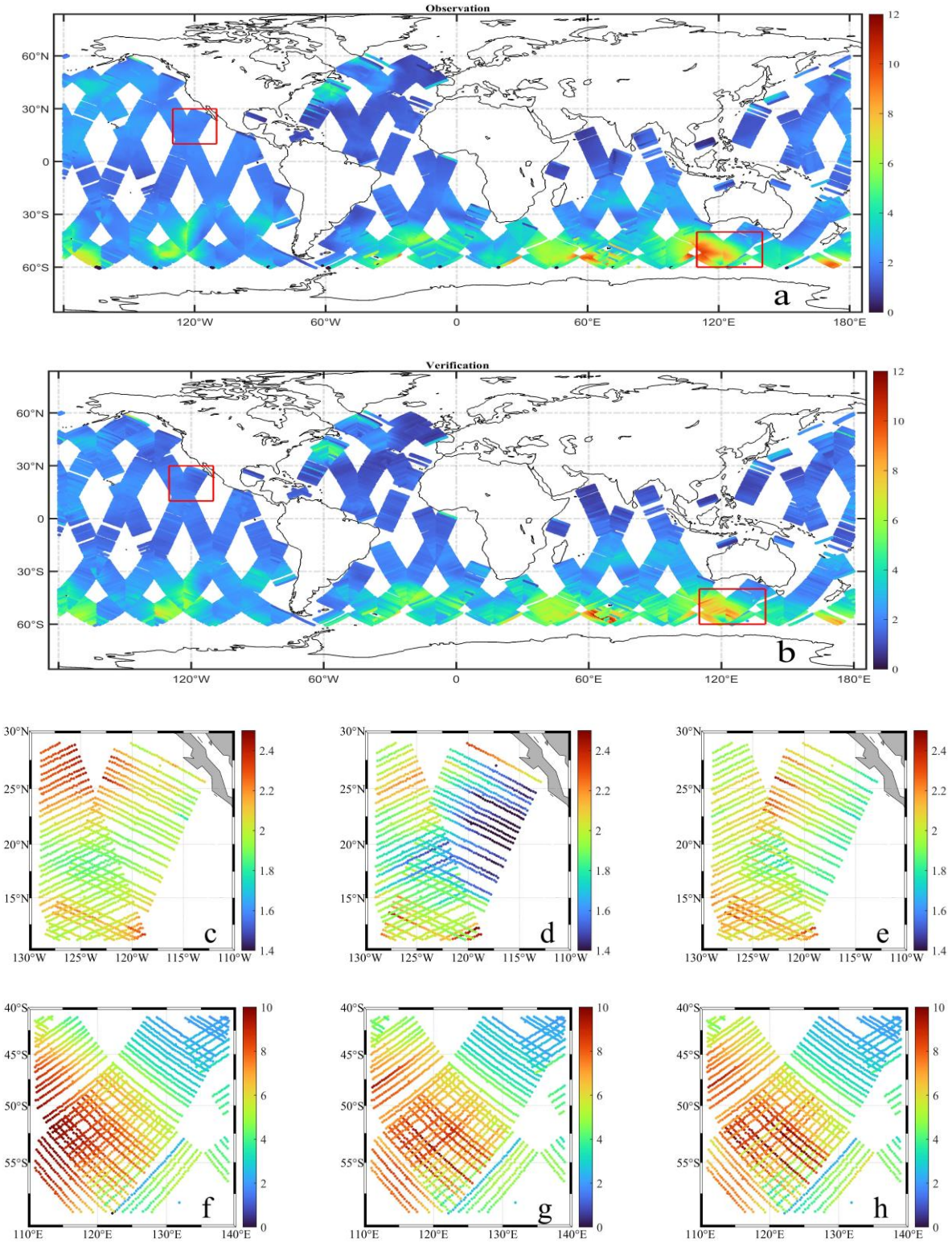

Figure 5 The results of the wide swath SWH. The observation (a) and the verification (b) of global wide swath SWH in Experiment 1, and the observation (c, f) and the verification (d and g in Experiment 1, as well as e and h in Experiment 2) of their magnitude plots in northwestern area and southeastern area (the red boxes in a and b), respectively.

From **Figure 5a**, it can be found that the data are distributed with a high probability between 1 and 5 m, and the values are generally larger than 5 m around 60° S. Numerical change in **Figure 5b** is basically consistent with the observations in **Figure 5a**. Two regions located in the northwest (130-110° W, 10-30° N) and southeast (110-140° E, 60-40° S) are drawn to manifest the detailed value intervals of wide swath SWH, respectively. **Figure 5d and e** fluctuate in a small range and the former has a difference of approximately 0.3 m compared to **Figure 5c**. Besides, the latter demonstrates a high consistency with **Figure 5c**. Combining with **Figure 5f**, **Figure 5g** exhibits a better performance than **Figure 5h** at larger values, which coincides with the phenomena reflected in **Figure 4b**. **Figure 5g** declares the expansion of the nadir SWH to generate a real-time grid product with wide swath along track, which can be employed as input for wave assimilation, spatial-temporal forecasting, extreme analysis and so on. Of course, it is undeniable that additionally considering swell into the input characteristics has a promising result when real-time is not strictly required. Furthermore, compared with **Figure 1**, our results extend the width of SWH to half of the wind field dimension, which demonstrates the effectiveness and feasibility of the model.

4 Conclusions

This paper employs the HY-2C data with simultaneously acquired wind and wave to build a deep learning model, the GRU approach, obtaining a wide swath SWH field along track. The Ku-band nadir SWH, as well as its latitude and longitude from altimeter are extracted to select the wind columns whose width occupy half of the scatterometer wind field dimension. The SWH of ERA5 is configured based on a time difference of half an hour and a spatial difference within 100 km. The validation data are segmented at a length of 300 and the center column outperformed the leftmost and rightmost columns under arbitrary interval, where the leftmost and rightmost columns are generally underestimated and slightly overestimated at the peaks and the troughs of wide swath SWH, respectively. The validation set with the length of 1-day at 10-second intervals is fed into the trained model, and the results show that a better fit appears, considering the swell to the input in the amplified northwestern area from 1.4 to 2.5 m. While in the southeast, its SWH ranges from 0 to 10 m and the model performs well without the swell feature for SWH larger than 7 m. When the data acquired by HY-2C are adopted as features and the data from ERA5 are utilized as the labels, a more time-sensitive grid product along track is generated. Nevertheless, when the data collected by HY-2C and the swell from ERA5 are applied as features, superior validation results are produced. Besides, the width of the SWH is extended to half of the wind field dimension, which could be further expanded or updated employing deep learning methods according to demands of the practical situation. The correlative wave parameters may be added appropriately to provide certain relevant information for the training model, so as to generate better grid products.

Data Availability Statement

The altimeter and scatterometer data of HY-2C can be obtained through osdds-ftp.nsoas.org.cn from National Satellite Ocean Application Service. The authors thank the Climate Data Store for providing the abundant high-quality ERA5 data, and these wave measurements can be downloaded from the ERA5 website (cds.climate.copernicus.eu).

Acknowledgments

We thank the National Satellite Ocean Application Service for providing the HY-2C altimeter and scatterometer data (accessible at osdds-ftp.nsoas.org.cn). We would also like to thank the Climate Data Store for the data from ERA5 (accessible at cds.climate.copernicus.eu). This work was supported by the National Natural Science Foundation of China [grant number 42176011]; the Shandong Provincial Natural Science Foundation [grant number ZR2020MD060]; the Fundamental Research Funds for the Central Universities [grant number 19CX05003A-5]. The authors declare no conflict of interest.

References

Guenaydin, K. (2008). The estimation of monthly mean significant wave heights by using artificial neural network and regression methods. *Ocean Engineering*, *35*(14-15), 1406-1415. https://doi.org/10.1016/j.oceaneng.2008.07.008

Lin, Y. P., Huang, C. J., & Chen, S. H. (2020). Variations in directional wave parameters obtained from data measured using a GNSS buoy. *Ocean Engineering*, *209*, 107513. https://doi.org/10.1016/j.oceaneng.2020.107513

Kang, J., Mao, R., Chang Y., & Fu, H. (2021). Comparative analysis of significant wave height between a new Southern Ocean buoy and satellite altimeter. *Atmospheric and Oceanic Science Letters*, *14*(C3), 100044. https://doi.org/10.1016/j.aosl.2021.100044

Dobson, E., Monaldo, F. & Goldhirsh J. (1987). Validation of Geosat altimeter-derived wind speeds and significant wave heights using buoy data. *Journal of Geophysical Research Oceans*, 1987, *92*(C10), 10719-10731. https://doi.org/10.1029/JC092iC10p10719

Durrant, T. H., Greenslade, D. J. M., & Simmonds, I. (2009). Validation of Jason-1 and Envisat Remotely Sensed Wave Heights. *Journal of Atmospheric and Oceanic Technology*, *26*(1), 123-134. https://doi.org/10.1175/2008JTECHO598.1

Bhowmick, S. A., Sharma, R., Babu, K. N., et al. (2015). Validation of SWH and SSHA from SARAL/AltiKa Using Jason-2 and In-Situ Observations. *Marine geodesy*, *38*, 193-205. https://doi.org/10.1080/01490419.2015.1042602

Kumar, U. M., Swain, D., Sasamal, S. K., Reddy, N. N., & Ramanjappa, T. (2015). Validation of SARAL/AltiKa significant wave height and wind speed observations over the North Indian Ocean. *Journal of Atmospheric and Solar-Terrestrial Physics*, *135*, 174-180. https://doi.org/10.1016/j.jastp.2015.11.003

Sepulveda, H. H., Queffeulou, P., & Ardhuin, F. (2015). Assessment of SARAL/AltiKa Wave Height Measurements Relative to Buoy, Jason-2, and Cryosat-2 Data. *Marine Geodesy*, *38*(sup1), 449-465. https://doi.org/10.1080/01490419.2014.1000470

Yang, J., & Zhang, J. (2019). Validation of Sentinel-3A/3B Satellite Altimetry Wave Heights with Buoy and Jason-3 Data. *Sensors*, *19*(13), 2914. https://doi.org/10.3390/s19132914

Yang, J., Zhang, J., Jia, Y., Fan, C., & Cui, W. (2020). Validation of Sentinel-3A/3B and Jason-3

Altimeter Wind Speeds and Significant Wave Heights Using Buoy and ASCAT Data. *Remote Sensing*. *12*(13), 2079. https://doi.org/10.3390/rs12132079

Chen, C., Zhu, J., Lin, M., Zhao, Y., Huang, X., & Wang, H., et al. (2013). The validation of the significant wave height product of HY-2 altimeter–primary results. *Acta Oceanologica Sinica*, *32*(011), 82-86. https://doi.org/10.1007/s13131-013-0381-6

Wang, J., Zhang, J. & Yang, J. (2013). The validation of HY-2 altimeter measurements of a significant wave height based on buoy data. *Acta Oceanologica Sinica*, *32*(011), 87-90. https://doi.org/10.1007/s13131-013-0382-5

Zhang H., Qing W. U., & Chen G. (2015). Validation of HY-2A Remotely Sensed Wave Heights against Buoy Data and Jason-2 Altimeter Measurements. *Journal of Atmospheric & Oceanic Technology*, *32*(6), 150402094232008. https://doi.org/10.1175/JTECH-D-14-00194.1

Wang, J., Aouf, L., Jia, Y., et al. (2020). Validation and Calibration of Significant Wave Height and Wind Speed Retrievals from HY2B Altimeter Based on Deep Learning. *Remote Sensing*, *12*, 2858. https://doi.org/10.3390/rs12172858

Liang, G., Yang, J., Wang J. (2021). Accuracy Evaluation of CFOSAT SWIM L2 Products Based on NDBC Buoy and Jason-3 Altimeter Data. *Remote Sensing*, *13*(5), 887. https://doi.org/10.3390/rs13050887

Li, X., Xu, Y., Liu, B., Lin, W., He, Y., & Liu, J. (2021). Validation and calibration of Nadir SWH Products from CFOSAT and HY-2B with satellites and in situ observations. J*ournal of Geophysical Research: Oceans*, *126*, e2020JC016689. https://doi.org/10.1029/2020JC016689

Zhang, L., Zhang, L., & Du, B. (2016). Deep Learning for Remote Sensing Data: A Technical Tutorial on the State of the Art. *IEEE Geoscience and Remote Sensing Magazine*, *4*, 22-40. https://doi.org/10.1109/MGRS.2016.2540798

Bentes, C., Velotto, D. & Lehner, S. (2015). Target classification in oceanographic SAR images with deep neural networks: Architecture and initial results. *IEEE International Geoscience and Remote Sensing Symposium* , 3703-3706, https://doi.org/10.1109/IGARSS.2015.7326627

Shen, D., Liu, B. & Li, X. (2019). Sea Surface Wind Retrieval from Synthetic Aperture Radar Data by Deep Convolutional Neural Networks. *IEEE International Geoscience and Remote Sensing Symposium*, 8035-8038. https://doi.org/10.1109/IGARSS.2019.8898542

Qin, T., Jia, T., Feng, Q., & Li, X. (2021). Sea surface wind speed retrieval from Sentinel-1 HH polarization data using conventional and neural network methods. *Acta Oceanologica Sinica*, *40*(1), 13-21. https://doi.org/10.1007/s13131-020-1682-1

Wang, J. K., Aouf, L., Dalphinet, A., Zhang, Y. G., Xu, Y., Hauser, D., & Liu, J. Q. (2021). The Wide Swath Significant Wave Height: An Innovative Reconstruction of Significant Wave Heights from CFOSAT's SWIM and Scatterometer Using Deep Learning. *Geophysical Research Letters*, *48*, e2020GL091276. https://doi. org/10.1029/2020GL091276

Wang, J. K., Aouf, L., Dalphinet, A., Li, B. X., Xu, Y., & Liu, J. Q. (2021). Acquisition of the significant wave height from CFOSAT SWIM spectra through a deep neural network and its impact on wave model assimilation. *Journal of Geophysical Research: Oceans*, *126*, e2020JC016885. https:// doi.org/10.1029/2020JC016885

Pang, D. & Tao, W. (2016). HY-2B and HY-2C Operational Satellites Under Development. *Aerospace China*, *17*(01), 69-69. https://doi. org/CNKI:SUN:ZGHA.0.2016-01-016

Ren Yueming. (2020). LM-4B Successfully Launched HY-2C Satellite. *Aerospace China*, *21*(03), 56. https://doi. org/CNKI:SUN:ZGHA.0.2020-03-011

Jia, Y., Lin M., & Zhang Y., (2020). Evaluations of the Significant Wave Height Products of HY-2B Satellite Radar Altimeters, *Marine Geodesy*, *43*(4), 396-413,

https://doi.org/10.1080/01490419.2020.1750513

Wang, Z., Zou, J., Stoffelen, A., Lin, W., Verhoef, A. et al., (2021). Scatterometer Sea Surface Wind Product Validation for HY-2C, *IEEE Journal of Selected Topics in Applied Earth Observations and Remote Sensing*, *14*, 6156-6164. https://doi.org/10.1109/JSTARS.2021.3087742

Hersbach, H., Bell, B., Berrisford, P., et al., (2020). The ERA5 global reanalysis. *Quarterly Journal of the Royal Meteorological Society*, *146*(730), 1999–2049. https://doi.org/10.1002/qj.3803